Surface smoothness of plasma-deposited amorphous silicon thin films: Surface diffusion of radical precursors and mechanism of Si incorporation

Mayur S. Valipa, Tamas Bakos, and Dimitrios Maroudas*
Department of Chemical Engineering, University of Massachusetts, Amherst, Massachusetts 01003-3110, USA
(Received 27 January 2006; revised manuscript received 16 June 2006; published 20 November 2006)

We present a detailed analysis of the fundamental atomic-scale processes that determine the surface smoothness of hydrogenated amorphous silicon (a-Si:H) thin films. The analysis is based on a synergistic combination of molecular-dynamics (MD) simulations of radical precursor migration on surfaces of a-Si:H films that are deposited computationally using MD simulation with first-principles density functional theory (DFT) calculations on the hydrogen-terminated Si(001)-(2×1) surface. The surfaces of the MD-grown a-Si:H films are remarkably smooth, as the mobile precursor, the SiH_3 radical, diffuses fast and incorporates in surface valleys. Analysis of the MD simulations of SiH_3 radical migration on a-Si:H surfaces yields an effective diffusion barrier of 0.16 eV. The low diffusion barrier on the a-Si:H surface is attributed to SiH_3 migration through overcoordinated surface Si atoms, where the radical remains weakly bonded to the surface at all times and does not break any strong Si-Si bonds along its migration pathway. Furthermore, the diffusing SiH_3 radical incorporates into the a-Si:H film only when it transfers an H atom and forms a second Si-Si backbond. On *rough* a-Si:H films, such H transfer from diffusing SiH_3 radicals is more likely to occur in surface valleys, even when the dangling bond (DB) density is low and DBs are not present in surface valleys. In addition, this H-transfer process is thermally activated with activation energy barriers (E_a) over the range 0.29–0.65 eV; E_a is determined by the Si-Si interatomic distance between the Si of the SiH_3 radical and the surface Si atom to which the H is transferred. The preferential incorporation in valleys is explained by both the increased residence time of the migrating precursor in valleys and the decreased activation barrier for incorporation reactions occurring in valleys. The mechanism and activation barrier for the H-transfer reaction on the a-Si:H surface were validated by performing first-principles DFT calculations on the crystalline Si surface.

DOI: 10.1103/PhysRevB.74.205324 PACS number(s): 68.55.Jk

I. INTRODUCTION

Thin films of hydrogenated amorphous silicon (a-Si:H) are grown typically by plasma-assisted deposition from silane (SiH_4) containing discharges. The film surface roughness influences the optical and electronic properties of the a-Si:H films, which in turn determine the performance of a-Si:H thin films in photovoltaic and optoelectronic device fabrication technologies.[1–3] Smooth surface morphologies are desirable for device-quality plasma-deposited a-Si:H films. The rate of diffusion on the growth surface of deposition precursors that are generated in the plasma determines the surface roughness of a-Si:H films. Device-quality a-Si:H films are deposited under conditions where the SiH_3 radical is the dominant deposition precursor.[4] The remarkable conformity and smoothness of device-quality a-Si:H films[5–8] grown under these conditions is used to conclude that the SiH_3 radical is very mobile on the a-Si:H surface[5,9] and can passivate dangling bonds (DBs) present in surface valleys of rough a-Si:H films during diffusion,[7] leading to surface smoothening.

Nevertheless, on a-Si:H surfaces, DBs are distributed randomly on both hills and valleys,[10] and the DB surface coverage is low ($\sim$0.001).[11,12] Hence, if surface smoothening was governed only by the location of DBs on the a-Si:H surface, the diffusing SiH_3 radical would be expected to passivate preferentially the DBs present in surface valleys over those DBs present on surface hills. In addition, the SiH_3 radical would be expected to migrate on the a-Si:H surface until it locates and passivates a DB present in a valley, although the DB surface coverage is very low. The likelihood of alternate modes of Si incorporation into the a-Si:H film excluding the involvement of the DBs, however, is high considering the low DB density on the a-Si:H surface, which is incompatible with the observed high film growth rates.[13]

Experimental data for the roughness evolution of a-Si:H films provide only indirect interpretations for the smoothening mechanism[14–18] and yield controversial results for the diffusion barrier of the SiH_3 radical on the a-Si:H surface.[14,15,19,20] The nature of the surface smoothening process is inferred indirectly from measurements of the static and dynamic scaling exponents, α and β, respectively, of the root mean squared surface roughness distribution, based on the assumption that the growth surface possesses a self-affine or self-similar topography.[14–16,18] The experimentally observed temperature-dependent decrease of β reveals only that the smoothening mechanism crosses over various universality classes of surface growth, where diffusion of some surface adsorbed species is present.[15,17]

In experimental studies of a-Si:H film surface evolution, additional models for surface diffusion, like the solid-on-solid model,[15] or assumptions such as that of a weakly adsorbed precursor state,[16] or of a self-similar surface morphological evolution[14] typically need to be invoked to connect measured data for the surface topography to kinetic parameters. Although there is general agreement that the adsorbed SiH_3 radical is the diffusing species, reported barriers for precursor diffusion on a-Si:H surfaces are dependent on the model employed and vary between 0.2 eV (Ref. 14) and $\sim$1 eV.[15] In addition, density functional theory (DFT) calcu-

lations performed on the hydrogen-terminated crystalline Si(110) surface have been used to propose the existence of a mobile state of the adsorbed SiH_3 radical, in which the radical diffuses with an energy barrier of 0.4 eV between nearest-neighbor surface Si atoms on this crystalline surface.[21] In spite of the above studies, the precise role of the SiH_3 radical precursor in determining the surface smoothness of a-Si:H films has remained unresolved because the atomic-scale mechanisms underlying radical precursor diffusion, as well as Si incorporation into the film, are not well understood and the activation barriers of the corresponding mechanistic steps remain undetermined.

In this article, we focus on analysis of the atomic-scale mechanisms underlying SiH_3 radical migration on *smooth* a-Si:H films, as well as incorporation of the SiH_3 radical in *rough* a-Si:H films, during radical diffusion on the a-Si:H surface, as identified by molecular-dynamics (MD) simulations, and their implications for a-Si:H surface smoothening. Our analysis is based on a synergistic combination of MD simulations for mechanistic understanding of the underlying dynamical phenomena with targeted first-principles DFT calculations for a better quantitative understanding of the mechanistic steps involved and their energetics. Specifically, numerous MD trajectories are generated for individual SiH_3 radical impingement events on *smooth* as well as *rough* a-Si:H surfaces. On the *smooth* surfaces, analysis of the MD-generated trajectories yields an average diffusion barrier of approximately 0.16 eV for SiH_3 diffusion on a-Si:H growth surfaces. Also, the analysis reveals that SiH_3 radical migration on the a-Si:H surface is mediated largely by surface overcoordination defects; there exists a mobile diffusion state of the SiH_3 radical where the DB of the radical binds to a fourfold coordinated surface Si atom, which, as a result of the radical's attachment, becomes fivefold coordinated. On the *rough* a-Si:H surfaces, detailed statistical analysis of the MD trajectories is performed to identify mechanisms of Si incorporation on the a-Si:H surface. The analysis reveals that the SiH_3 radical incorporates preferentially in valleys of the rough a-Si:H surface morphology, even in the absence of DBs in the valley. The radical incorporation mechanism consists of transfer of an H atom from the diffusing SiH_3 radical in conjunction with formation of a second Si-Si backbond between the radical and the surface that leads to the immobilization of the radical. The activation energetics for radical incorporation depends on the interatomic distance between the radical's Si and the surface Si to which the H atom is transferred. This dependence together with the high residence time of the radical in surface valleys favors radical incorporation in the valleys.

The article is structured as follows. The computational methods employed for MD simulation, SiH_3 radical trajectory generation, as well as DFT calculation of reaction pathways are presented in Sec. II. In Sec. III, SiH_3 radical migration trajectories are analyzed on smooth a-Si:H surfaces to elucidate the mechanism of radical diffusion, and determine the corresponding activation energy barrier; the dependence of the barrier on the local atomic structure in the vicinity of the radical adsorption site on the a-Si:H surface, as well as experimental data for radical migration on the a-Si:H surface also are discussed in Sec. III. In Sec. IV, representative SiH_3 radical migration trajectories on rough a-Si:H surfaces are analyzed and the mechanisms, dynamics, and energetics of the corresponding H-transfer reactions that lead to preferential Si incorporation in surface valleys are reported. Results from statistical analysis of the MD-generated radical migration trajectories also are reported in Sec. IV, together with analysis of activation energetics for H transfer and Si incorporation and its dependence on the local structure in the vicinity of the reaction event. Results from DFT calculations for the corresponding Si incorporation reaction on a crystalline Si surface are reported in Sec. V. The implications of the H-transfer reaction as the predominant Si incorporation mechanism mediating the a-Si:H surface smoothening phenomena are discussed in the context of experimental results for the a-Si:H growth process in Sec. VI. Finally, the conclusions of our study are summarized in Sec. VII.

II. COMPUTATIONAL METHODS

The a-Si:H films used in this study were prepared over the temperature (T) range $475\ \mathrm{K} \leqslant T \leqslant 800\ \mathrm{K}$ by MD as described in Refs. 22 and 23. Specifically, we have modeled the deposition of a-Si:H films at substrate temperatures of 500 K and 773 K by MD on initially H-terminated Si(001)-(2×1) substrate surfaces through repeated impingement of SiH_3 radicals as the sole deposition precursor for durations up to 5 ns.[23] Our MD simulation supercell contains typically over 850 atoms, ranging from 520 atoms at the beginning of deposition to 860 atoms after deposition by MD for 5 ns. A typical film thickness at the end of the growth duration of 5 ns was approximately 15 Å. Although the a-Si:H film was deposited on a c-Si substrate, structural characterization of the MD-deposited a-Si:H film established that the film was fully disordered;[24] this disordered film structure is reflected, e.g., on the Si-Si pair correlation function for the a-Si:H film, which exhibits *only* the first two peaks corresponding to the first two coordination shells, characteristic of an amorphous material with *only* short-range order, i.e., with the long-range order of the crystalline structure being completely lost.

Detailed structural characterization of the surfaces of a-Si:H films grown for durations of 1 ns and 2 ns at 500 K and 773 K revealed that the corresponding a-Si:H films exhibited rough surface morphologies during early stages of film growth, whereas a-Si:H films deposited for 5 ns were remarkably smooth,[9] indicating that the a-Si:H films smoothen during the course of the deposition process. Subsequently, we conducted four runs of 150 SiH_3 radical impingement events at $T=475$, 500, and 525 K and at $T=750$, 773, and 800 K on the surfaces of a-Si:H films that were grown for durations of 5 ns and thermally annealed at the growth temperatures of 500 K and 773 K, respectively; these growth runs resulted in the generation of four smooth a-Si:H films for every T.[22] In the MD simulations, the interatomic interactions were described by Tersoff's potential for silicon as extended by Ohira and co-workers to include Si-H, H-H, and the corresponding three-body interactions.[25,26] A complete description of the interatomic potential functional form and set of parameters, an assessment of its predictive capabilities for radical-surface interactions for both ordered and

a-Si:H surfaces, as well as the numerical integration scheme used in our MD simulations, have been reported elsewhere.[23,27] Comparisons of the MD-grown films with experimentally deposited a-Si:H films[28,29] showed good agreement for the surface hydride compositions, H coverage, and surface smoothness.[23,30] The potential also has predicted successfully H-induced disorder-to-order transitions leading to crystallization of a-Si:H films to form nanocrystalline silicon.[31]

For analysis of SiH_3 radical migration on smooth a-Si:H films, at every T, we used the four smooth a-Si:H films obtained as a result of the film growth simulations over the temperature range 475 K$\leqslant T \leqslant$800 K. Subsequently, each of the four a-Si:H films was equilibrated by thermally annealing the a-Si:H films through MD for 120 ps at the respective temperatures. The duration of the annealing period was chosen to allow for sufficient surface relaxation, as reflected by the equilibration of the total system energy for all of the atoms in the MD supercell. We studied the diffusion mechanism of the SiH_3 radical on our thickest a-Si:H films with smooth surfaces so as to allow for suitable comparisons with experimental data on precursor diffusion that are reported for thick, smooth a-Si:H films. To provide statistically significant results, we generated six MD trajectories of SiH_3 radical migration after impinging on the surface for each of the four smooth a-Si:H films at a particular T, sampling random impingement locations on the a-Si:H surface. Hence, we generated 24 MD trajectories of radical migration for each substrate temperature. The duration of each trajectory was chosen to be 120 ps, allowing for sufficient monitoring of the radical's migration dynamics over the surface areas employed in the simulation;[23] no other radicals were impinged on the surface during this period, ruling out mutual interaction with other impinging radicals. Also, we have analyzed the mechanism of SiH_3 radical migration by studying bond-forming and bond-breaking processes along the migration trajectory, as well as by determining the coordination number of the Si atom of the radical and the surface Si atoms to which it is bonded, along the migration pathway. The Si-Si bond length is used in determining the coordination of the Si atoms. Specifically, the maximum allowed interatomic distance for Si-Si bond formation is specified by the extent of the first coordination shells in the a-Si:H film, as determined by the location of the first minimum after the first peak in the corresponding Si-Si pair correlation function, $g(r)$; for the potential employed in this study, this distance ranges from 2.75 to 2.85 Å over the temperature range examined.

To study atomic-scale processes that are responsible for the surface smoothening of a-Si:H films during deposition, we have generated 154 MD trajectories of SiH_3 radical impingement and subsequent migration on rough a-Si:H surfaces and monitored the radical throughout the duration of the MD trajectories. The number of radical migration trajectories that we analyzed was chosen to provide a sufficiently large sample for statistically significant analysis of Si incorporation events on the four rough growth surfaces examined, i.e., after 1 ns and 2 ns of growth simulation for the a-Si:H films deposited at 500 K and 773 K. The duration of the MD-generated SiH_3 surface migration trajectories at 773 K was chosen to be 80–150 ps, while the trajectories at 500 K were chosen to be 200–400 ps in duration; these time periods allowed for sufficient monitoring of the radical's migration dynamics over the surface areas ($\sim$5 nm^2) employed in the simulation and facilitated the observation of thermally activated H-transfer events, as described in detail in Sec. IV. No other radicals were impinged on the surface during this period, ruling out mutual interaction with other subsequently impinging radicals. The Si incorporation reaction energetics was obtained through energy minimization along the corresponding reaction paths using a conjugate gradient minimization algorithm.[23]

In addition, DFT calculations for H transfer from the SiH_3 radical were performed on the H-terminated Si(001)-(2×1) crystalline surface for a targeted quantitative analysis of the mechanism and activation barrier for the incorporation reaction identified on the a-Si:H surface; the choice of surface sites for reaction analysis was made using information obtained from analysis of reaction pathways identified by MD and is discussed in Sec. IV. Our DFT calculations were implemented within the generalized gradient approximation (GGA) (Ref. 32) and employed slab supercells,[33] plane-wave basis sets,[33] and ultrasoft pseudopotentials.[34] Fully optimized migration pathways were constructed by employing the nudged elastic band (NEB) method that included a climbing image[35] to obtain saddle-point configurations and activation barriers. The progress of the radical migration was monitored by visualizing planar intersections of the three-dimensional valence electron density (VED) distribution along the hopping pathway; the VED maps provide detailed information about the occurrence of bond-breaking and bond-forming events. Our DFT calculational methodology has been described in detail in Ref. 36.

III. ANALYSIS OF SiH_3 RADICAL MIGRATION ON SMOOTH a-Si:H SURFACES

In our MD analysis of SiH_3 radical migration on smooth a-Si:H surfaces, the location of the center of mass of the SiH_3 radical on the a-Si:H surface, as well as the atomic coordination of the SiH_3 radical's Si atom and of the surface Si atoms to which the radical is bonded during diffusion, are monitored throughout the duration of each radical migration trajectory. The mobility of the SiH_3 radical is determined through the evolution of the mean squared displacement (MSD), $\langle \Delta \mathbf{r}^2 \rangle$, of the radical's center of mass. The MSD is expressed through an Einstein equation as

$$\langle \Delta \mathbf{r}^2(t) \rangle \equiv \langle [\mathbf{r}(t) - \mathbf{r}(0)]^2 \rangle = 6Dt, \tag{1}$$

for three-dimensional motion, where $\mathbf{r}(t)$ is the center-of-mass position of the diffusing species at time t, the angular brackets denote ensemble averaging, and D is the diffusion coefficient,

$$D = D_0 \exp(-E_a/kT). \tag{2}$$

In Eq. (2), E_a denotes the average activation energy barrier for radical diffusion. The long-time slope of the MSD evolution yields D, according to Eq. (1), and an Arrhenius plot of D versus T according to Eq. (2) yields E_a. In implement-

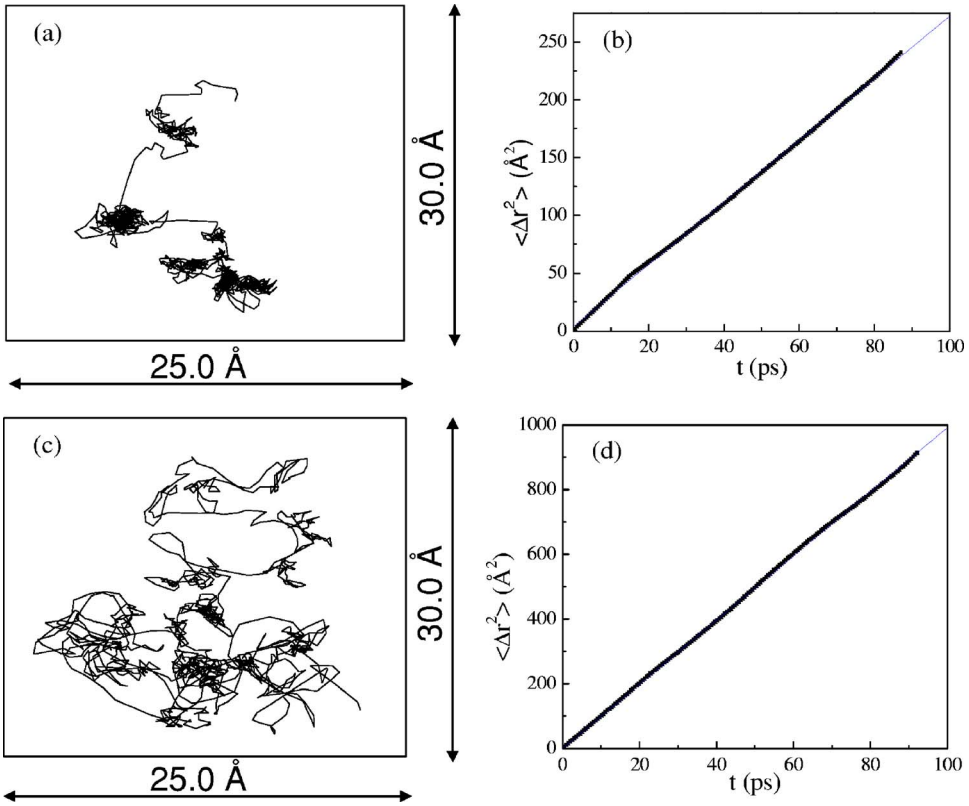

FIG. 1. (Color online) Representative MD-generated SiH_3 radical surface migration trajectories (a) and (c), and evolution of the radical's mean squared displacement (b) and (d), for smooth a-Si:H surfaces at 500 K and 773 K, respectively. In (b) and (d), the blue straight line is a fit to the MD results shown as black dots.

ing Eq. (1), we perform ensemble averaging for the MSD calculation by choosing multiple origins (>50), each separated by 0.5 ps along the MD trajectory, to maximize the utilization of the complete MD trajectory.[37] Therefore, E_a represents an average activation energy barrier for radical diffusion over the T range 475 K$\leqslant T\leqslant$800 K. The use of the proportionality factor 6 in Eq. (1) originates from expressing Δr^2 as $\Delta r^2=\Delta x^2+\Delta y^2+\Delta z^2$, where the surface plane is the Cartesian xy plane, i.e., including any radical migration normal to the (average) surface plane; as a result, the complexity of the local amorphous surface morphology is taken into account and the radical displacement is resolved into components along all the three Cartesian axes accordingly.

Figures 1(a) and 1(c) show representative MD trajectories on the smooth a-Si:H surfaces at 500 K and 773 K, respectively, while Figs. 1(b) and 1(d) show the evolution of the corresponding (ensemble averaged) MSDs for these MD trajectories. Comparison of Fig. 1(a) with Fig. 1(c) shows that the SiH_3 radical is more localized on the a-Si:H surface at 500 K than at 773 K; at the higher T, the radical is more mobile and diffuses randomly over a larger area on the a-Si:H surface. The differences in mobility of the SiH_3 radical at 500 K and 773 K are quantified by the MSD plots shown in Figs. 1(b) and 1(d), respectively; the slope of the MSD evolution in Fig. 1(d) is approximately four times greater than that in Fig. 1(b). Furthermore, as a result of the ensemble averaging, the linear fit for the MSD evolution is excellent.

The diffusion coefficient at each T, $D(T)$, is obtained by averaging over all of the 24 MD trajectories of radical surface migration at each T. The resulting Arrhenius plot is shown in Fig. 2; this Arrhenius plot yields an E_a for SiH_3 radical diffusion on the smooth a-Si:H surface of 0.16±0.01 eV, with a prefactor $D_0=(1.82\pm0.07)\times10^{-3}$ cm^2/sec. To our knowledge, this is the first direct calculation of E_a for SiH_3 surface diffusion on a-Si:H films reported in the amorphous silicon literature. Several groups have reported an $E_a\sim0.15-0.30$ eV for SiH_3 diffusion on thick, smooth a-Si:H films through either indirect measurements[14,19] or calculations.[20] Typically, these indirect approaches combine experimental measurements with models that assume certain kinetics for the underlying mechanisms.[14,19,20] For example, Bray and Parsons reported an E_a of 0.20 eV using time-dependent surface topography and dynamic scaling models for a-Si:H,[14] while Maeda and co-workers assumed a simplified set of reactions to explain the H concentration in a-Si:H films produced by rf glow discharges of SiH_4 and calculated an E_a of 0.30 eV.[20] The

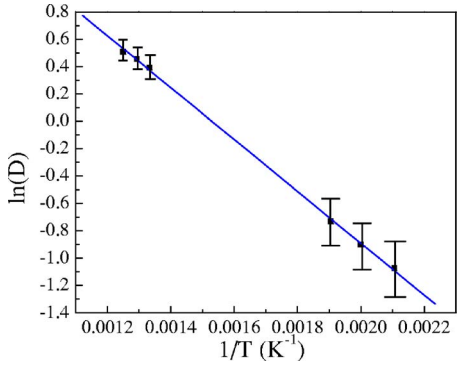

FIG. 2. (Color online) Arrhenius plot for the temperature (T) dependence of the SiH_3 radical diffusivity on smooth a-Si:H surfaces over the T range 475 K$\leqslant T\leqslant$800 K.

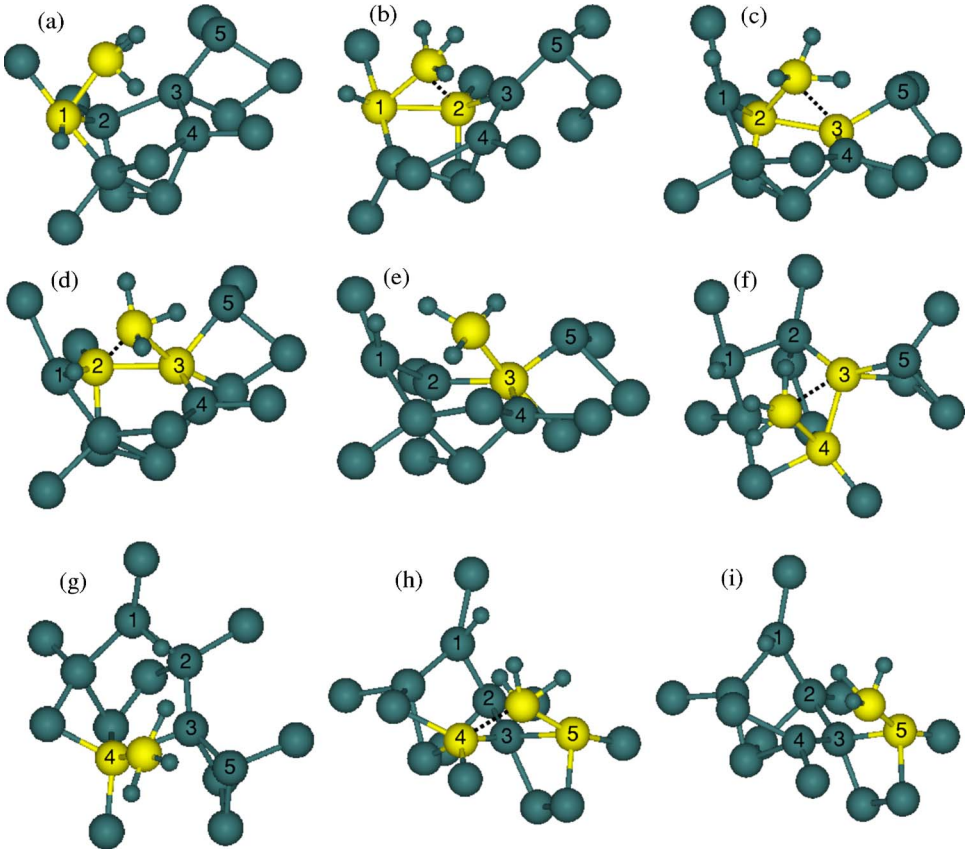

FIG. 3. (Color online) A representative SiH_3 radical hopping sequence chosen from a 120-ps-long migration trajectory on an a-Si:H surface at 773 K. In the atomic clusters shown, the Si of the radical and the surface Si atoms to which it is bonded are shown as yellow spheres, while the neighboring Si and H atoms are indicated by large and small green spheres, respectively. H atoms of the radical also are shown as small green spheres. In the sequence of snapshots (a)–(i), the SiH_3 radical hops sequentially from the surface Si atom labeled "1" to the one labeled "5."

calculated value of 0.16 eV from our MD simulations is consistent with (within the range of) the above indirect experimental results.

Our analysis also reveals that the surface Si atom to which the SiH_3 radical is bonded is typically fivefold coordinated and, consequently, the radical-surface interaction is weakened. During migration, the SiH_3 radical breaks easily its weak Si-Si bond with the surface Si atom and hops to an adjacent surface Si atom that again becomes fivefold coordinated as a result of its bonding with the radical's Si; in the transition state, the radical is bonded to both the surface Si atoms that it hops between. The overcoordination of surface Si atoms is due to the diffusing radical and this "overcoordinated state" accompanies the radical along its pathway. The radical continues its migration on the a-Si:H surface in this manner until it incorporates into the film. Therefore, we attribute the low barrier for SiH_3 surface diffusion to the weak adsorption onto the a-Si:H surface of the SiH_3 radical and to its migration predominantly through overcoordination defects.

To elucidate further the mechanism of radical diffusion on the a-Si:H surface, a representative sequence of radical hopping events chosen from a 120-ps-long trajectory on the a-Si:H surface is shown in Fig. 3. Typically, the surface Si atom to which the radical is bonded is fivefold coordinated during the radical's migration as shown in Figs. 3(a), 3(e), and 3(g); as a result, the radical-surface Si-Si bond is weak. During migration, the SiH_3 radical breaks easily its weak bond with the Si atom labeled "1" and hops to an adjacent Si atom labeled "2," as shown in Fig. 3(c); in the intermediate state, the radical also is fivefold coordinated and weakly bonded to the Si atom labeled "2," as shown by the dotted line in Fig. 3(b). In a similar manner, the SiH_3 radical hops from the Si atom labeled "3" in Fig. 3(e) to the Si atom labeled "4" in Fig. 3(g), while the radical is fivefold coordinated in the intermediate state, as shown by the weak bond in Fig. 3(f). In the final configuration shown in Fig. 3(i), the radical has hopped to the Si atom labeled "5," which possesses a dangling bond (DB). Therefore, the SiH_3 radical diffuses on the a-Si:H surface until it passivates a DB; subsequently, it remains localized in the vicinity of the surface Si atom possessing the DB. However, passivation of a surface Si DB by the migrating SiH_3 radical is not a strict requirement for the termination of the migration sequence and incorporation of the radical into the film; it is typically the case on surfaces of smooth a-Si:H films. The radical incorporation mechanism on rough a-Si:H films is analyzed systematically in Sec. IV.

To analyze the effect of the local atomic structure and atomic coordination at the a-Si:H surface on the mechanism and energetics of radical diffusion, we monitored the Si-Si interatomic distances between the radical's Si atom and the surface Si atoms to which the radical is bonded during the radical hopping event. Also, we calculated the average coordination number, $\langle Z \rangle$, of the radical's Si atom and the surface Si atoms during radical diffusion over the temperature range $475\ \mathrm{K} \leqslant T \leqslant 800\ \mathrm{K}$. These values have been averaged over eight 120-ps-long MD trajectories for each temperature.

Figure 4 gives a schematic representation of a radical hopping event on the a-Si:H surface, where the Si atom of the radical is labeled "1" and the surface Si atoms between which the radical hops are labeled "2" and "3," respectively.

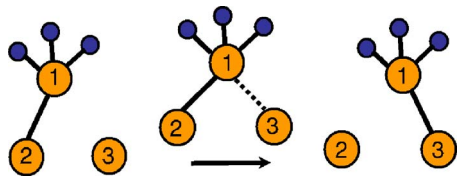

FIG. 4. (Color online) Schematic representation of radical hopping on the a-Si:H surface. The Si of the radical and the surface Si atoms to which it is bonded are shown as orange spheres, while the H atoms of the radical are shown as blue spheres.

In Table I, we have listed the average coordination numbers of the radical's Si atom and the surface Si atoms, as well as the Si-Si interatomic distances involved in the intermediate configuration shown in Fig. 4 over the temperature range examined. From the data of Table I, the average coordination number of the radical's Si atom and the surface Si atoms over the T range 475 K$\leqslant T \leqslant$800 K are 4.57 and 4.82, respectively, averaged over eight MD trajectories for each T, and are practically independent of T. Therefore, on average, the surface Si atoms that are bonded to the radical are nearly fivefold coordinated, leading to a weak Si-Si bond with the radical's Si atom. As noted earlier, the overcoordination of surface Si atoms is due to the diffusing radical and this "overcoordinated state" accompanies the radical on its diffusion pathway.

In addition, we have calculated the two Si-Si interatomic distances between the radical's Si atom and the surface Si atoms, as well as the Si-Si interatomic distance between the two surface Si atoms labeled "2" and "3," in the intermediate configuration of Fig. 4. The radical is bonded to both of the surface Si atoms in the intermediate configuration, as seen from the average Si-Si interatomic distances, $d_{\mathrm{Si1\text{-}Si2}}$ and $d_{\mathrm{Si1\text{-}Si3}}$, in Table I, which indicate that the radical is bonded weakly to the surface; however, one of the radical-surface Si-Si bonds is stronger than the other, as seen in Table I. Most importantly, the radical has not broken any bonds and is bonded to the surface in the intermediate configuration. In Table I, the Si-Si interatomic distance, $d_{\mathrm{Si2\text{-}Si3}}$, between the surface Si atoms indicates that the two Si atoms are typically not separated by distances in excess of 3.5 Å, so that the radical's Si atom does not have to strain its bond with the surface substantially in order to hop from one surface Si atom to another. Hence, the radical can remain bonded to the surface throughout its migration pathway, and it does not break any Si-Si bonds. The weak adsorption of the SiH_3 radical onto the a-Si:H surface, its migration predominantly through overcoordination defects, as well as the continuous bonding of the radical with the surface throughout the diffusion pathway, are the key factors that account for the low diffusion barrier that is calculated based on the MD trajectories.

In addition, we have performed high-accuracy DFT calculations for the surface migration of the SiH_3 radical, employing a crystalline Si (c-Si) surface as a model for the local bonding environment of the a-Si:H surface.[38] Among the various radical migration pathways investigated on the Si(001)-(2×1):H surface, one pathway that bears particular significance to SiH_3 radical diffusion on the a-Si:H surface involves SiH_3 radical migration along the dimer rows, in the trough between adjacent dimer rows. In this migration pathway, the radical always stays bonded to the surface; the Si atom of the radical bonds to surface Si atoms that are already fourfold coordinated and they become fivefold coordinated as a result of the radical's attachment to the surface. For this radical hopping step, the DFT analysis yields an activation barrier of 0.18 eV.[38] We conclude that the E_a calculated on the a-Si:H surface (0.16 eV) is in good agreement with the DFT result. It is important to note that, for this radical hopping step on a crystalline Si surface, the local atomic structure in the vicinity of the SiH_3 radical is similar to that observed on the a-Si:H surface during SiH_3 radical migration: in this sense (similarity in local atomic structure), a link is established between the MD-based diffusion study on the a-Si:H surface and the quantitatively accurate DFT calculation of radical hopping on the ordered Si surface.

IV. ANALYSIS OF SiH_3 RADICAL MIGRATION AND Si INCORPORATION ON ROUGH a-Si:H FILM SURFACES

The surface smoothening mechanism of a-Si:H consists of two key steps: rapid radical diffusion, followed by the subsequent incorporation of the SiH_3 radical on the a-Si:H surface. In the previous section, we analyzed the SiH_3 radical diffusion mechanism on surfaces of smooth a-Si:H films. In

TABLE I. Temperature dependence of the average coordination numbers, $\langle Z\rangle_{\mathrm{radical}}$ and $\langle Z\rangle_{\mathrm{surface}}$, for the radical's Si atom and the surface Si atoms that are bonded to the radical, respectively, as well as the interatomic distances $d_{\mathrm{Si1\text{-}Si2}}$, $d_{\mathrm{Si1\text{-}Si3}}$, and $d_{\mathrm{Si2\text{-}Si3}}$ between the Si atoms labeled "1" (radical) and "2," "1" and "3," and "2" and "3," respectively, in the intermediate configuration of Fig. 4. At each temperature, the listed values have been averaged over eight 120-ps-long MD trajectories.

T (K)	$\langle Z\rangle_{\mathrm{radical}}$	$\langle Z\rangle_{\mathrm{surface}}$	$d_{\mathrm{Si1\text{-}Si2}}$ (Å)	$d_{\mathrm{Si1\text{-}Si3}}$ (Å)	$d_{\mathrm{Si2\text{-}Si3}}$ (Å)
475	4.54±0.02	4.88±0.11	2.48±0.09	2.58±0.06	3.45±0.60
500	4.58±0.02	4.92±0.16	2.47±0.09	2.57±0.06	3.44±0.61
525	4.54±0.03	4.90±0.11	2.46±0.09	2.57±0.06	3.44±0.59
750	4.63±0.04	4.78±0.14	2.46±0.11	2.59±0.08	3.35±0.60
773	4.57±0.06	4.79±0.09	2.46±0.11	2.59±0.08	3.37±0.59
800	4.55±0.03	4.67±0.16	2.46±0.11	2.59±0.08	3.36±0.59

this section, we analyze the SiH_3 radical incorporation mechanism, during radical migration on surfaces of *rough* a-Si:H films. The center-of-mass location of the SiH_3 radical on rough a-Si:H surfaces, as well as the atomic coordination of the SiH_3 radical's Si atom and of the surface Si atoms to which the radical is bonded during its diffusion, were monitored throughout the duration of each radical migration trajectory. Our MD trajectories revealed that, in all cases examined, the diffusing SiH_3 radical incorporates into the a-Si:H film only when it transfers an H atom and forms a Si-Si backbond. The transferred H atom can then either be abstracted by SiH_3 to form an SiH_4 molecule that returns to the gas phase[36,39,40] or diffuse into the bulk a-Si:H film,[41] while the Si atom of the radical is rendered immobile (incorporation) at the site of the H transfer reaction. Therefore, the location on the rough a-Si:H surface topography of the H-transfer reaction assumes great significance for the evolution of the surface roughness. Interestingly, our MD simulations indicate that H transfer from diffusing SiH_3 radicals occurs more frequently in surface valleys, leading to preferential Si incorporation in such valleys. The observed SiH_3 radical migration trajectories can be classified into several categories based on the local atomic coordination in the vicinity of the H-transfer event. Specifically, three basic types of H-transfer events were identified:

(i) in a surface valley, the SiH_3 radical transfers an H atom to a surface Si atom that is bonded to the SiH_3 radical's Si atom and the Si-Si bond between the radical's Si and the surface Si breaks after H transfer;

(ii) in a surface valley, the SiH_3 radical transfers an H atom to a surface Si atom that is not bonded to the radical's Si atom and is typically a second-nearest neighbor of the radical's Si atom; and

(iii) on a surface hill, the SiH_3 radical transfers an H atom to a surface Si atom that is a second-nearest neighbor of the radical's Si atom.

Henceforth, we will denote the above classes of reactions as reaction type 1, 2, and 3, respectively. Detailed structural and energetic analyses are presented for one trajectory that is representative of each reaction type. The detailed dynamics of the H-transfer reaction are discussed only for one trajectory that is classified under reaction type 1. The role of the H-transfer reaction in mediating the surface-smoothening phenomena is discussed for all cases.

A. Reaction type 1

In this reaction type, the radical diffuses on the rough a-Si:H surface until it transfers one of its H atoms to a surface Si atom that is bonded weakly to the Si atom of the SiH_3 radical; the weak Si-Si bond between the radical and the surface Si to which the H atom is transferred breaks after H transfer, while the Si of the radical forms another Si-Si backbond with the surface and is incorporated into the a-Si:H film. Figure 5(a) shows the surface morphology, with the evolving radical's center-of-mass trajectory superimposed for a case leading to an H-transfer reaction classified under reaction type 1. We use a similar representation for all of the trajectories that are discussed subsequently in this article. The radical is impinged on a hill of the a-Si:H film that was deposited for 2 ns of growth simulation time at 500 K; the radical impingement location is indicated in Fig. 5(a). After some migration in the hill area, the radical migrates to a valley and remains localized in the valley, as seen clearly in Fig. 5(a). In the valley, the radical transfers an H atom to a surface Si atom while breaking a weak Si-Si backbond with the surface Si receiving the transferred H, it forms another Si-Si backbond, and it is incorporated in the surface valley. The incorporation is shown by the strong localization of the radical migration trajectory in the valley in Fig. 5(a), indicating the practical immobilization of the radical in the vicinity of the H-transfer location.

Figures 5(b)–5(d) show optimized configurations of atomic clusters chosen from the vicinity of the reaction site. Figure 5(b) shows that in state *A* (initial state prior to H transfer), the SiH_3 radical is adsorbed on the surface by the formation of a direct Si-Si bond between the radical and a surface Si atom labeled "1"; in addition, the radical is weakly bonded to another surface Si atom labeled "2" (denoted here by Si2). In the transition state, TS, one of the H atoms of the SiH_3 radical occupies an asymmetric, weak bond-centered-like configuration,[42] where it is bonded weakly to both the Si atom of the SiH_3 radical and Si2, as shown in Fig. 5(c); the weak Si-Si bond between the Si of the radical and Si2 is broken in the TS, and the Si of the radical forms another Si-Si backbond with a surface Si atom labeled "3" (denoted here by Si3). In the final configuration *B*, the H atom is transferred to Si2 with which it forms a strong Si-H bond, while the Si of the radical has formed two Si-Si backbonds and is incorporated in the surface valley. Two structural aspects of this H-transfer reaction are particularly important: the H atom is transferred from the SiH_3 radical only when the Si of the radical becomes fivefold coordinated in state *A*, and, more importantly, the H atom is not transferred to a dangling bond in state *B*; note that Si2 is fourfold coordinated in state *A*.

During SiH_3 diffusion on the a-Si:H surface, the radical samples many surface sites by hopping from one surface Si atom to another; the radical remains bonded to one surface Si atom, which then becomes fivefold coordinated, similar to Si1 in Fig. 5(b). However, frequently, the radical itself moves within interaction range of another neighboring surface Si atom and forms a weak fifth bond with the surface Si. In such a state, the Si of the radical contains a floating bond such as, for example, the weak fifth bond between the SiH_3 and Si2 in Fig. 5(b). In this state (*A*), if one of the H atoms of the SiH_3 radical, which was just outside interaction range of a surface Si atom, moves within interaction range of that Si atom, a competition ensues between the Si of the radical and the surface Si atom for bonding with this H atom; for example, in the above reaction, Figs. 5(b)–5(d), Si2 competes with the radical's Si atom for the yellow-colored H atom, as seen in the TS, Fig. 5(c). Subsequently, the H atom occupies a bond-center-like position between the radical and the surface Si atom, as shown in Fig. 5(c), before the H atom is bonded with the surface Si atom as seen in Fig. 5(d). It is important to note that the H atom can be transferred easily, only when the Si of the radical becomes fivefold coordinated, so that the corresponding Si-H bonds are rendered

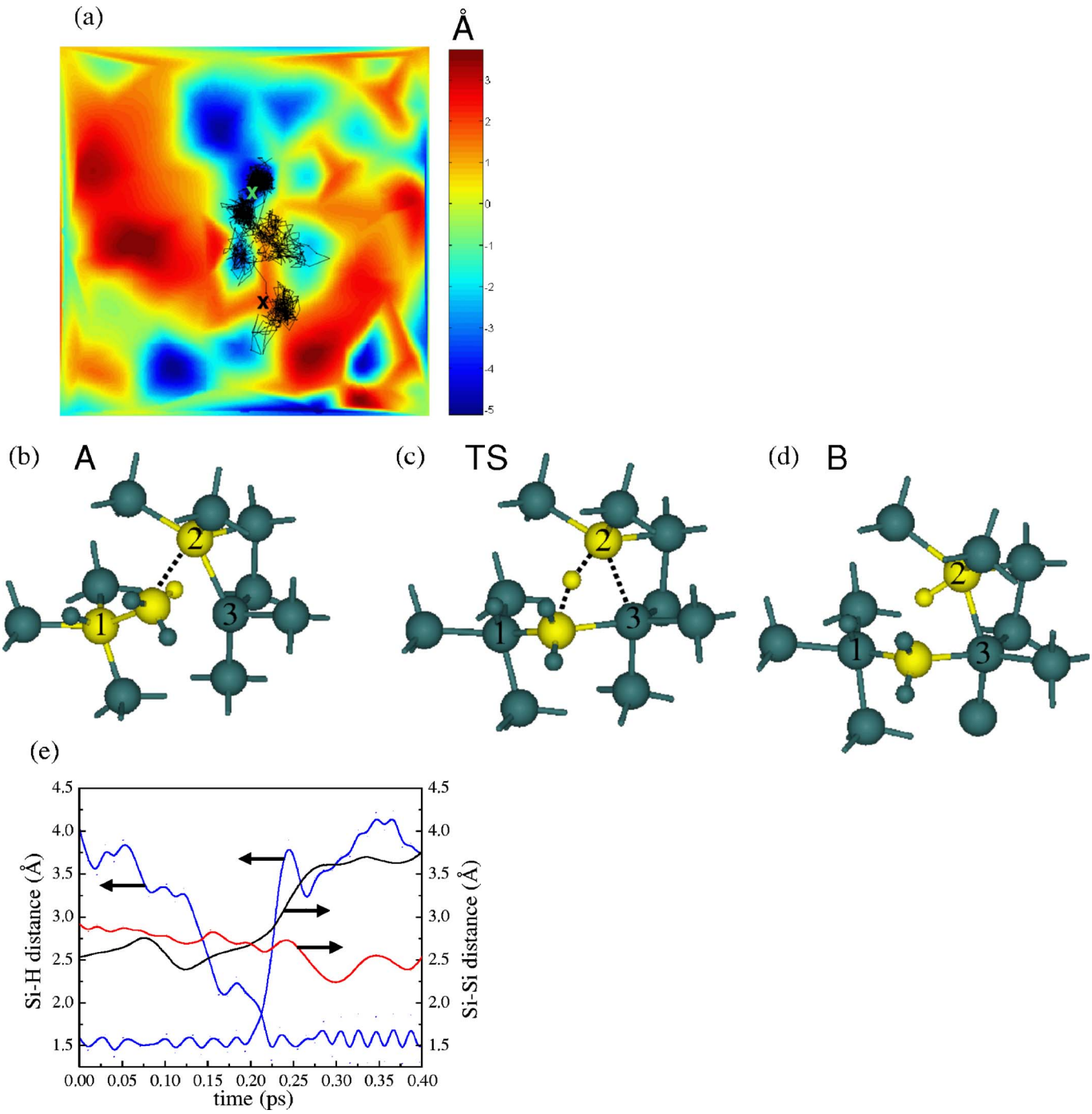

FIG. 5. (Color online) (a) Surface morphology of a rough a-Si:H film at 500 K, with the radical's center-of-mass trajectory (solid line) superimposed for a 265-ps-long SiH_3 radical migration trajectory that is classified under reaction type 1. The surface area shown is 21.7×21.7 Å^2. Dark-blue surface regions correspond to valleys in the surface topography. × (black) indicates the radical impingement location and × (gray) indicates the H-transfer location on the a-Si:H surface. Optimized structure of (b) the initial (*A*), (c) intermediate (TS), and (d) final (*B*) atomic configurations for the H-transfer reaction occurring at the surface location indicated in Fig. 1(a). In the atomic clusters shown, the Si atom of the radical and the surface Si atom to which the H is transferred are shown as large yellow spheres, while the neighboring Si atoms are shown as large green spheres. The transferred H atom is shown as a small yellow sphere. Dotted lines indicate weak bonds. (e) Evolution, during the course of the H-transfer reaction, of the Si-Si and the Si-H interatomic distances between the two Si atoms (the radical's Si and Si2) and the H atom participating in the reaction. The Si-Si interatomic distance evolution between the radical's Si and surface atom Si3 also is shown in (e) (red curve) indicating the formation of the second Si-Si backbond (between the radical's Si and Si3; the first one is formed between the radical's Si and Si1).

weaker than the normal Si-H bonds in an SiH_4 molecule. After H transfer from the SiH_3 radical, the Si of the radical can form strong Si-Si backbonds and incorporate into the a-Si:H film, as seen clearly in Fig. 5(d). The Si of the radical is then rendered immobile (to within atomic vibrations), as the Si atom now has to break two strong Si-Si backbonds before it can hop from one Si to another on the a-Si:H surface. Essentially, the Si atom of the original SiH_3 radical becomes analogous to the Si atom of an "immobile" SiH_2 radical, after the H-transfer event, leading to formation of an adsorbed dihydride species on the surface.

Importantly, the H atom is not transferred to a Si atom with a DB; instead, Si2 is fourfold coordinated prior to H transfer, and becomes fivefold coordinated after H transfer as shown in Fig. 5(d). This creates a floating bond for Si2, so that the transferred H atom can hop again from Si2 to another surface Si atom. As a result, the transferred H atom diffuses on the a-Si:H surface through floating bonds until it passivates a DB; once the H atom passivates a DB, it becomes localized until the floating-bond-mediated H diffusion process resumes. Such a diffusion mechanism for H in a-Si:H has been observed both in classical[41,43] and in *ab initio*[44] MD simulations of H migration in a-Si:H. Therefore, the above mechanism results in Si incorporation in the valleys, even in the absence of DBs in the valleys.

This H-transfer reaction depicted in Figs. 5(b)–5(d) is thermally activated with an activation energy barrier, E_a, of 0.65 eV and is endothermic by 0.02 eV. It should be noted, however, that unlike crystalline Si, a-Si:H is characterized by a *distribution* of bond lengths and bond angles. Consequently, the local structure around each H-transfer site is generally different and, therefore, the reaction energetics could vary for different Si-Si bonds on the a-Si:H surface. Detailed analysis of the MD trajectories reveals that E_a is dependent primarily on the interatomic distance between the Si atom of the radical and the surface Si atom to which the H is transferred, $d_{\text{Si-Si}}$, immediately prior to the H-transfer event. The specific H-transfer reaction discussed above represents an extreme case with the highest E_a and the strongest Si-Si bond ($d_{\text{Si-Si}}$=2.57 Å) among all the reactions that were classified under migration type 1. More detailed analysis on the range of E_a can be found in Sec. IV D.

Finally, the evolution of the Si-Si and Si-H bond lengths during the course of the specific reaction, Figs. 5(b)–5(d), is shown in Fig. 5(e). The reaction occurs at approximately 0.2 ps for the portion of the MD trajectory shown in Fig. 5(e). Before H transfer, the Si-Si bond formed between the radical's Si and Si2 is strained, while this Si-Si bond is broken after the H-transfer reaction, as shown in Fig. 5(e). The Si-Si interatomic distance evolution between the radical's Si and surface atom Si3 also is shown in Fig. 5(e) indicating the formation of the second Si-Si backbond between the radical's Si and Si3. For reactions within this category (type 1), E_a is reduced with increasing Si-Si bond strain, as it is easier to break a more strained Si-Si bond.

B. Reaction type 2

In this reaction type, the diffusing SiH_3 radical transfers an H atom to a surface Si atom that is typically a second-nearest neighbor of the radical's Si atom, and Si incorporation occurs in a surface valley, after the Si of the radical forms another Si-Si backbond. Figure 6(a) shows the surface morphology, with the evolving radical's center-of-mass trajectory superimposed for a representative case leading to an H-transfer reaction classified under reaction type 2. The radical is impinged on a hill of the a-Si:H film that was deposited for 1 ns of growth simulation time at 500 K; the radical impingement location is indicated in Fig. 6(a). The radical is very mobile on the hill and diffuses rapidly toward a valley; subsequently, the radical trajectory remains localized in the valley, as shown in Fig. 6(a). Again, the SiH_3 radical transfers an H atom to a surface Si atom, after the radical samples surface sites in the valley; the Si of the radical forms another Si-Si backbond, and is incorporated in the valley, which is shown by the strong localization of the MD trajectory in the vicinity of the H-transfer location in the valley in Fig. 6(a). Figures 6(b)–6(d) show optimized configurations of atomic clusters chosen from the vicinity of the reaction site. Figure 6(b) shows that in state *A*, the Si atom of the SiH_3 radical is fivefold coordinated due to its weak bonding with the surface Si atom labeled "3"; in this state, the yellow H atom is not bonded with the surface Si atom labeled "2," and the SiH_3 radical's Si atom is a second-nearest neighbor of Si2. In the transition state TS, the H atom moves within interaction range of Si2 and forms a bond-centered-like configuration, where it is bonded weakly to both the Si atom of the SiH_3 radical and Si2, as shown in Fig. 6(c). In the final configuration, *B*, the H atom is transferred to Si2, while the Si of the radical has formed another Si-Si backbond with Si3 and is incorporated in the surface valley. Again, there are no DBs involved in this H-transfer process. The corresponding E_a for this reaction is 0.36 eV. The activation barrier for this reaction is lower than that observed for the reaction discussed in Sec. IV A, as there was no Si-Si bond to be broken between the radical's Si and Si2 in the initial configuration, and $d_{\text{Si-Si}}$ was 3.10 Å.

C. Reaction type 3

In this reaction type on the a-Si:H surface, the diffusing SiH_3 radical transfers an H atom to a surface Si atom that is typically a second-nearest neighbor of the radical's Si atom and Si incorporation occurs on a surface hill, after the Si of the radical forms a Si-Si backbond. Figure 7(a) shows the surface morphology, with the evolving radical's center-of-mass trajectory superimposed for a representative case leading to an H-transfer reaction classified under this reaction type. The radical is impinged on a hill of the a-Si:H film deposited for 1 ns of growth simulation time at 500 K; the radical impingement location is indicated in Fig. 7(a). The radical is very mobile on the hill and samples many surface sites, prior to transferring an H atom to a surface Si atom. In this case, the Si of the radical is incorporated on the hill in the vicinity of the H-transfer location, as shown in Fig. 7(a), after the formation of another Si-Si backbond. Figures 7(b)–7(d) show optimized configurations of atomic clusters chosen from the vicinity of the reaction site. Figure 7(b) shows that in state *A*, the Si atom of the SiH_3 radical is

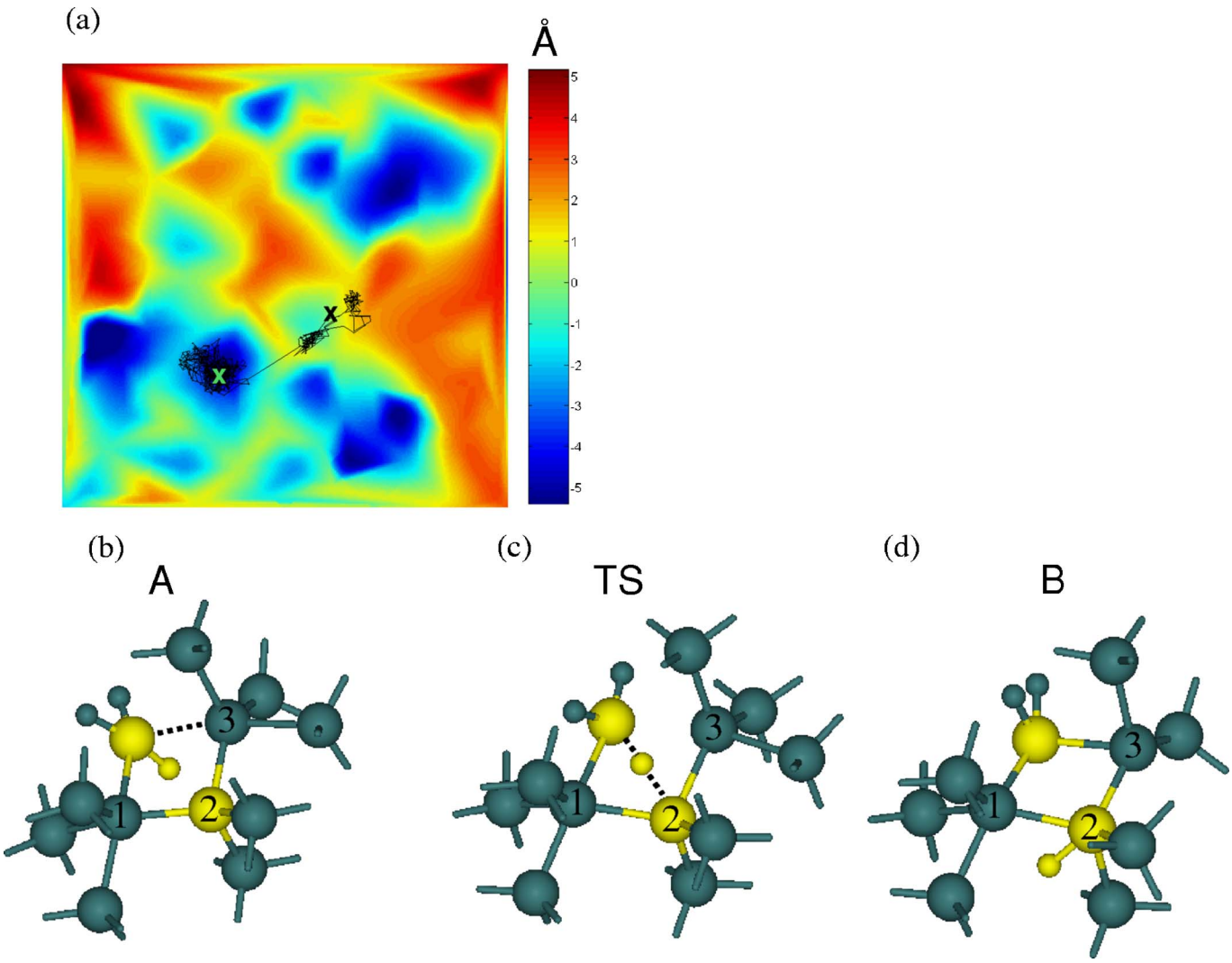

FIG. 6. (Color online) (a) Surface morphology of a rough a-Si:H film at 500 K, with the radical's center-of-mass trajectory (solid line) superimposed for a 325-ps-long SiH_3 radical migration trajectory that is representative of reaction type 2. The surface area shown is 21.7×21.7 Å^2. The notation used for the evolving trajectory on the a-Si:H surface is consistent with that of Fig. 5. Optimized structure of (b) the initial (A), (c) intermediate (TS), and (d) final (B) configurations for the H-transfer reaction occurring at the surface location indicated in Fig. 6(a). The coloring scheme for the various atoms in configurations A, TS, and B is consistent with that of Fig. 5.

fivefold coordinated due to its weak bonding with a surface Si atom, and the SiH_3 radical's Si atom is a second-nearest neighbor of the Si atom labeled "2." In the transition state TS, the H atom is bonded weakly to both the Si atom of the SiH_3 radical and Si2, as shown in Fig. 7(c). In the final configuration B, the H atom is transferred to Si2, while the Si of the radical has formed another Si-Si backbond with the surface Si atom labeled "3" and is incorporated on the surface hill. There are no DBs involved in this H-transfer process, as Si2 is fourfold coordinated prior to H transfer (in state A) as shown in Fig. 7(b). The corresponding E_a for this reaction is 0.57 eV. The E_a for this reaction is greater than that observed for the reaction discussed in Sec. IIIB, as the separation between the Si of the radical and Si2 was large ($d_{\text{Si-Si}}$=3.45 Å), and the Si-H bonds in the TS configuration are very strained.

D. Statistical analysis of the MD trajectories

Statistical analysis of the MD-generated SiH_3 radical migration trajectories is performed to obtain information on the topographical distribution of sites for Si incorporation on the a-Si:H surface. Furthermore, the analysis is used to determine the dependence of the E_a for H transfer and Si incorporation on the local atomic structure in the vicinity of the reaction event.

The analysis of the MD trajectories yielded that H transfer leading to Si incorporation on the a-Si:H surface occurs preferentially in surface valleys or at the edges of valleys in ~72% of the cases examined, while Si incorporation on surface hills occurs in only 28% of the 154 MD trajectories that were analyzed. H transfer to a dangling bond (leading to DB passivation) was observed to occur in less than 7% of the trajectories analyzed. Thus, the H-transfer reactions do not

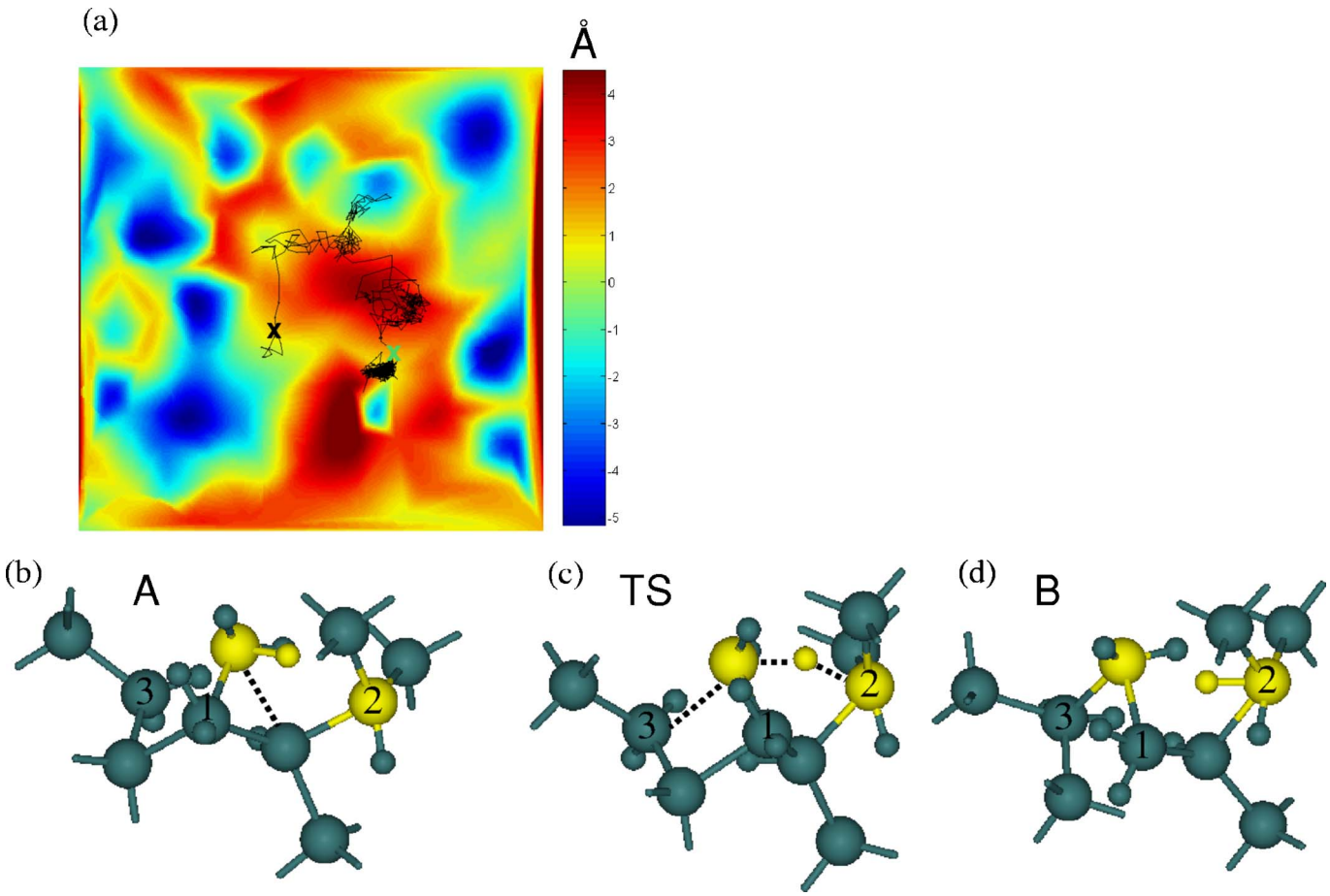

FIG. 7. (Color online) (a) Surface morphology of a rough a-Si:H film at 500 K, with the radical's center-of-mass trajectory (solid line) superimposed for a 200-ps-long SiH_3 radical migration trajectory that is classified under reaction type 3. The surface area shown is 21.7 $\times$21.7 Å^2. The notation used for the evolving trajectory on the a-Si:H surface is consistent with that of Fig. 5. Optimized structure of (b) the initial (*A*), (c) intermediate (TS), and (d) final (*B*) configurations for the H-transfer reaction occurring at the surface location indicated in Fig. 7(a). The coloring scheme for the various atoms in configurations *A*, TS, and *B* is consistent with that of Fig. 5.

require the presence of DBs and lead to valley filling even when the DB density is low and DBs are not present in surface valleys. One important reason for the preferential Si incorporation in valleys, is the long residence time of the SiH_3 radical in surface valleys: the SiH_3 radical was observed to migrate rapidly on the hills, but was observed typically to remain localized in many surface valleys (including the valley edges), as soon as it reaches surface valley regions during its diffusion on the a-Si:H surface. There is a strong driving force (local chemical potential gradient) for the radical to migrate from surface hills to valleys due to the surface Si-Si bond strain distribution as determined by the surface topography.[10] Once the radical reaches the valley, it remains localized in the valley, due to the absence of any strong strain-induced driving force to diffuse out of the valley. Therefore, the radical is better able to sample surface sites in the valleys, which may provide reactive sites for an H-transfer-mediated Si incorporation reaction, through the mechanistic pathways outlined in Secs. IV A and IV B.

To understand the effects of the local structural environment on the H-transfer processes and differentiate between such effects for Si incorporation reactions occurring on hills from those occurring in valleys, we constructed the distribution of $d_{\text{Si-Si}}$ for all of the 154 MD trajectories by grouping separately the H-transfer events occurring in the valleys from those on surface hills. The $d_{\text{Si-Si}}$ distributions for both valleys and hills exhibit multiple peaks:[38] the first is centered at $\sim$2.75 Å, corresponding to surface Si atoms that are first-nearest neighbors of the SiH_3 radical's Si atom forming a strained Si-Si bond with it, while the second one is centered at $d_{\text{Si-Si}} > 3.0$ Å, corresponding to surface Si atoms that are not bonded to the Si atom of the SiH_3 radical (typically, second-nearest neighbors of the radical's Si atom). The population of bonded neighbors of the radical is centered at a mean value, μ, of $d_{\text{Si-Si}}$ that is $\mu=2.75\pm0.09$ Å for the valleys and $\mu=2.74\pm0.08$ Å for the hills.[38] The population of second-nearest neighbors of the radical's Si is centered at $\mu=3.16\pm0.12$ Å for the valleys and at $\mu=3.46\pm0.25$ Å for the hills. Therefore, the population distributions of second-nearest neighbors varies significantly between hills and valleys; the mean value of $d_{\text{Si-Si}}$ for hills is 0.30 Å larger than that in the valleys, and the corresponding standard deviations for $d_{\text{Si-Si}}$ also are higher on the hills than in the valleys. This has important implications for the corresponding Si incorporation probabilities on the hills and in the valleys, as discussed below.

We chose also many H-transfer events that span a broad range of $d_{\text{Si-Si}}$, from the large sample of MD trajectories, to perform energetic analysis and derive the corresponding energy landscape along the reaction path. We found that there was a spectrum of activation energy barriers over the range 0.29–0.65 eV.[38] The barrier is high when $d_{\text{Si-Si}} < 2.65$ Å, as the Si-Si bond needs to be strained during H transfer from one Si atom to another, or when $d_{\text{Si-Si}} > 3.4$ Å, where the two Si atoms are far apart and the Si-H bond is very strained in the transition state.[38] Therefore, there exists a range, 2.7 Å $< d_{\text{Si-Si}} < 3.2$ Å that corresponds to low E_a ($\leqslant 0.4$ eV). On further analysis, we find that in surface valleys ~71% of the H-transfer reactions occur for 2.7 Å $< d_{\text{Si-Si}} < 3.2$ Å, which corresponds to $E_a \leqslant 0.4$ eV, whereas on surface hills only 42% of the H-transfer reactions occur in the same interval for $d_{\text{Si-Si}}$. However, on surface hills, ~34% of the H-transfer events occur for 3.2 Å $< d_{\text{Si-Si}} < 3.7$ Å (compared to only 9% in surface valleys), leading typically to $E_a > 0.5$ eV for Si incorporation on hills.[38] Therefore, on average, the activation barrier for Si incorporation is higher on surface hills than in surface valleys, which facilitates the valley filling mechanism by allowing for preferential incorporation of the radical precursor's Si in valleys. Such preferential incorporation of Si in the surface valleys of rough a-Si:H films is indeed reflected in our MD simulations, where less than 30% of the total Si incorporation events occurred on the hills.

Finally, we offer a qualitative interpretation for the distribution of the Si-Si interatomic distances, $d_{\text{Si-Si}}$, and its effects on the E_a values. The local environment in valleys is more advantageous for *H*-transfer reactions because more Si-Si distances fall in the range where the barrier for *H* transfer is low. The mean interatomic distance in the valleys is lower due to the local surface topology in the valley: surface valleys are concave, while surface hills are convex. This difference in surface curvature induces opposite types of Si-Si bond strain, namely tensile in hills and compressive in valleys, which affect accordingly (through activation strain) the corresponding activation barriers for reaction. This qualitative explanation is supported by the statistical (quantitative) data (MD results), which, in conjunction with the dependence of the E_a on $d_{\text{Si-Si}}$, ensures that the Si incorporation probability is higher in surface valleys than on hills.

V. DFT CALCULATION OF Si INCORPORATION

To achieve a better quantitative understanding of the mechanism and energetics of Si incorporation observed on the a-Si:H surface, we have performed high-accuracy DFT calculations for the H-transfer reaction, employing a crystalline Si surface as a model for the local bonding environment of the a-Si:H surface. These quantitative predictions validated the mechanistic picture that emerged from the analysis of the MD simulations. Specifically, we analyzed based on DFT an H-transfer-mediated Si incorporation reaction on the crystalline Si(100)-(2×1):H surface, along the low-barrier migration path of the SiH_3 radical in the trough along dimer rows.[38] The concave geometry of the dimerized surface trough mimics the typical local environment of a-Si:H surface valleys and offers candidate Si atoms (reactive sites) to which the diffusing radical may transfer one of its H atoms.

To capture the properties of an H atom transfer and simultaneous SiH_3 radical insertion (incorporation) reaction that resembles most closely the general mechanism identified on the a-Si:H surface, we start with an SiH_3 radical in its diffusive state,[38] i.e., in a configuration where the radical's Si is bonded to a fivefold coordinated surface Si atom, before hopping to an adjacent nearest-neighbor Si in the trough along the dimer row on the crystalline surface. The optimized atomic configurations along the H-transfer-reaction pathway together with the corresponding VED distributions are shown in Fig. 8. The initial state is represented by Fig. 8(a), where the surface Si atom, Si3, is fivefold coordinated (due to the adsorbed SiH_3 radical) and the local geometrical configuration is representative of the radical's diffusive state on the a-Si:H surface.

An analysis of the reaction pathway shows that two Si-Si bonds between the radical's Si atom and the surface form prior to H transfer. In this intermediate step, the radical's Si atom is fivefold coordinated, as shown in Fig. 8(d), which is an unstable state and results in an increase of the total energy of the surface. Immediately, an H atom from the SiH_3 radical begins to transfer to a nearby Si atom across the trough, Si2, as shown in Fig. 8(e), which results in a reduction of the total energy; Si2 is fourfold coordinated prior to H transfer and does not possess a DB. The interatomic distance between Si1 and Si2, $d_{\text{Si-Si}}$, immediately prior to H transfer, corresponds to $d_{\text{Si-Si}} = 3.66$ Å, as shown in Fig. 8(d). In the final stage of the H-transfer-mediated Si incorporation reaction, the H atom completes the transfer process to Si2 and Si1 has formed two strong Si-Si backbonds with the crystalline Si surface; the final state is shown in Fig. 8(f), where Si1 is immobilized on the crystalline surface. The Si1-Si2 distance first increases as the SiH_3 radical turns toward the dimer row, then decreases as the H is pulled to Si2 over the trough, and increases again as the final state relaxes.

The energetic progress along the reaction path is plotted in Fig. 9. The saddle point of the reaction corresponds to the H-transfer step. This H-transfer-mediated Si incorporation reaction has a barrier of 0.73 eV and is endothermic by 0.22 eV, as shown in Fig. 9. The corresponding dependence of E_a on $d_{\text{Si-Si}}$ is shown in Fig. 10 together with the MD results of Ref. 38. The smooth red curve shown in Fig. 10 has been fitted to the MD results and has been extrapolated over a broader $d_{\text{Si-Si}}$ range than that corresponding to the MD results; for the extrapolation, we used a seventh-order polynomial, a functional form that was found to minimize the error in the fitting of the MD results. The data point from the DFT calculation is placed at $d_{\text{Si-Si}} = 3.66$ Å and $E_a = 0.73$ eV on Fig. 10. As is evident from Fig. 10, there is an excellent agreement between the DFT-calculated E_a for H transfer from SiH_3 on the Si(001)-(2×1):H surface and the activation barrier extrapolated from the corresponding MD study on the a-Si:H surface. This agreement validates the mechanistic findings of the MD-based Si incorporation study performed on the a-Si:H surface. It should be mentioned that the pathway for the H-transfer reaction reported and discussed

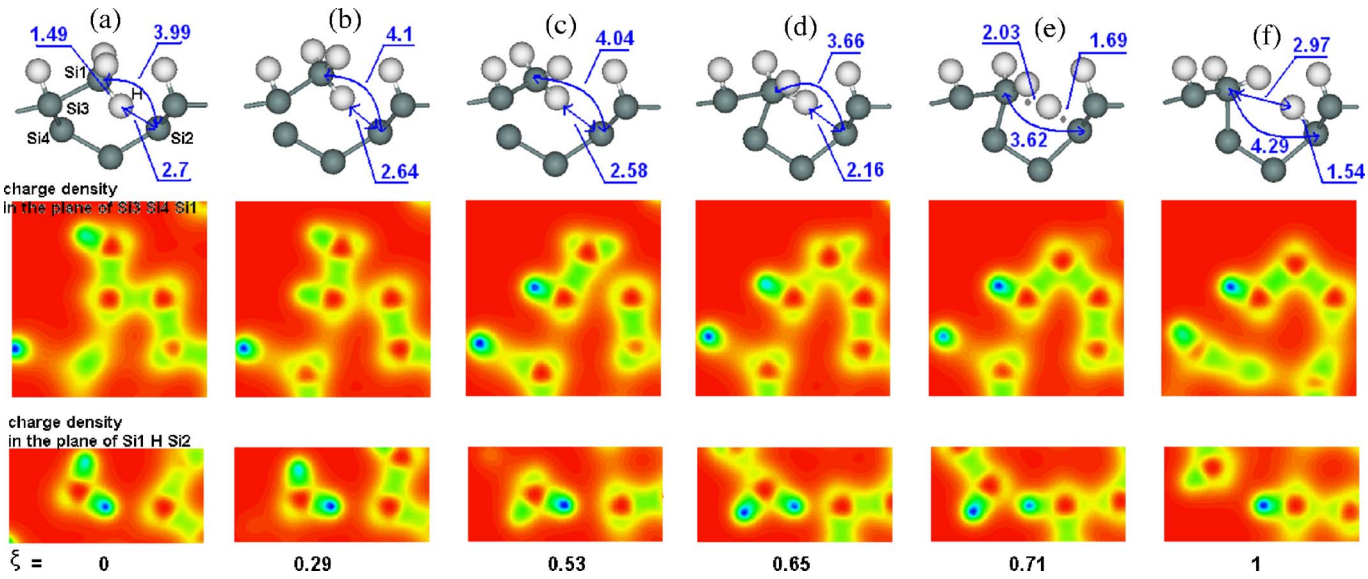

FIG. 8. (Color online) Reaction pathway of H-transfer-mediated Si incorporation on the Si(001)-(2×1):H surface. (a)–(f): Top: selected optimized atomic configurations along the reaction path. Only a small region of the surface cell is shown. Dark and white spheres denote Si and H atoms, respectively. Dotted lines indicate weak bonds. The numbers shown give the indicated interatomic distances in Å. Middle: valence electron density (VED) distribution in the plane of the three atoms Si1, Si3, and Si4, shown in (a). Bottom: VED distribution in the plane of the three atoms Si1, H, and Si2, shown in (a). Each VED map corresponds to the configuration directly above it in the top panel. Blue and red regions are characterized by high and low VED, respectively.

here based on our DFT analysis (Figs. 8 and 9) is the lowest-energy pathway for this reaction on the Si(001)-(2×1):H surface among all of the possible H-transfer pathways on this surface that also were examined in this study. In addition, the DFT study reveals that, most importantly, a fivefold coordinated Si atom (of the radical) needs to be created before H transfer from the SiH_3 radical can take place as shown in Fig. 8(d). After the Si atom of the SiH_3 becomes fivefold coordinated, H transfer from the radical to a surface Si atom is facilitated. This is fully consistent with the Si incorporation mechanism on the a-Si:H surface, where the H atom is transferred from the SiH_3 radical only when the Si of the radical becomes fivefold coordinated in state *A*, as shown in Figs. 4(b), 5(b), and 6(b). Therefore, for this H-transfer event on the crystalline Si surface, the local atomic structure in the vicinity of the SiH_3 radical, as well as the mechanistic details of the reaction, are similar to those observed on the a-Si:H surface during H-transfer-mediated Si incorporation: this establishes a link between the MD-based Si incorporation study on the a-Si:H surface and the quantitatively accurate DFT calculation for Si incorporation on the ordered Si surface.

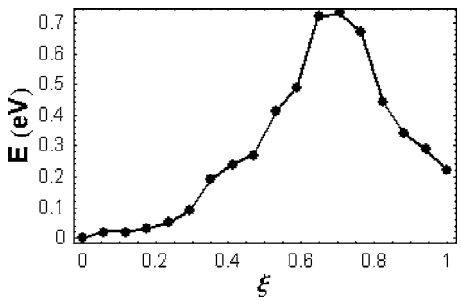

FIG. 9. Total energy, *E*, as a function of a properly defined reaction coordinate, ξ, along the H-transfer-mediated Si incorporation reaction path.

VI. DISCUSSION

The smoothening mechanism observed in our MD simulations has important implications for experimental growth processes of smooth a-Si:H films. Several experimental studies have addressed the roughness of a-Si:H films grown through plasma-assisted deposition, under conditions where

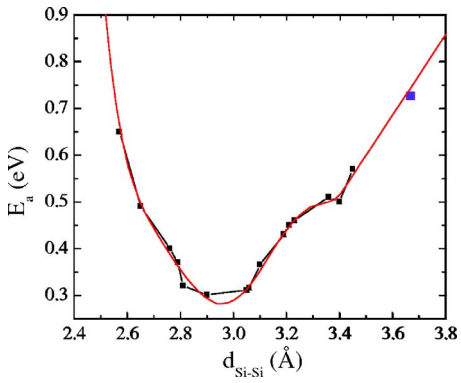

FIG. 10. (Color online) Dependence of E_a on $d_{\text{Si-Si}}$; the red curve has been fitted to the MD results (black filled squares) of Ref. 38 for the dependence of E_a on $d_{\text{Si-Si}}$ and has been extrapolated over a broader $d_{\text{Si-Si}}$ range than that corresponding to the MD results. The blue data point corresponds to the DFT calculation for H-transfer-mediated Si incorporation on the Si(001)-(2×1):H surface; the DFT-calculated E_a corresponds to the saddle-point energy of Fig. 9.

the dominant deposition precursor is the SiH_3 radical.[14–18] Smets and co-workers studied the scaling behavior of the surface morphology of a-Si:H films deposited from an SiH_3-dominated plasma using atomic force microscopy (AFM) and *in situ* spectroscopic ellipsometry, in conjunction with Monte Carlo simulations.[15] Their study reported a surface smoothening mechanism depending on temperature, T, with an activation energy barrier of $\sim$1.0 eV.[15] However, using time-dependent surface topography and dynamic scaling models to study surface transport kinetics during a-Si:H deposition, Bray and Parsons observed that surface transport is dominated by the diffusion of adsorbed species with an activation barrier of $\sim$0.20 eV.[14] Their results also indicated that the smoothening mechanism is only weakly thermally activated, as the roughening exponent, β, is virtually independent of T over the range 25 °C$<T<$100 °C. Kondo and co-workers performed an *ex situ* study of a-Si:H surface morphology using AFM over the range 50 °C$<T<$450 °C, and reported a weak dependence of the surface roughness evolution on T.[17] Finally, Tanenbaum and co-workers studied the morphology of plasma-deposited a-Si:H films using *ex situ* scanning tunneling microscopy and reported that chemical-potential-driven precursor diffusion to valleys is the dominant surface smoothening mechanism.[18]

However, the above experimental studies assumed that the only growth sites on the a-Si:H surface are DBs, and, therefore, these DBs should diffuse preferentially to surface valleys of a-Si:H for surface smoothening to occur. In the present article, we have shown that Si incorporation can occur preferentially in valleys even in the absence of DBs, and that DBs are not necessarily the only growth sites on the a-Si:H surface. Our studies indicate that surface smoothening is limited by Si incorporation in surface valleys with typical activation barriers of 0.3–0.4 eV, which is consistent with the kinetics of the smoothening process reported in Refs. 14 and 17. Nevertheless, we expect the activation barrier for H transfer to increase substantially for $d_{\text{Si-Si}}<2.6$ Å or $d_{\text{Si-Si}}>3.5$ Å, as seen by the extrapolation in the plot of Fig. 10, which could account for smoothening barriers on the order of 1 eV; in such cases, finer-scale experimental structural characterization would be required for direct comparisons with the experimental findings of Ref. 15. Based on our analysis, however, we expect either strained Si-Si bonds with $d_{\text{Si-Si}}>2.70$ Å, or surface Si atoms which are not bonded with the Si atom of the radical, with 2.8 Å$<d_{\text{Si-Si}}<3.2$ Å, to participate preferentially in the H-transfer reaction on the a-Si:H surface, rather than stronger, unstrained Si-Si bonds that would necessitate a higher activation energy for Si incorporation.

In Sec. III we showed that the SiH_3 radical migrates on the a-Si:H surface with an activation barrier of 0.16 ± 0.01 eV. Therefore, the activation barrier for radical migration on the a-Si:H surface is significantly lower than the E_a for Si incorporation. This barrier difference has important implications for the a-Si:H growth process and the experimentally observed temperature dependence of the a-Si:H surface roughness evolution. At a $T\sim300$ K, the SiH_3 radical is more likely to passivate a DB after migrating on the a-Si:H surface, rather than transfer an H atom in a valley, given the much lower activation barrier for radical surface migration. Since the DB distribution is random, this implies that at low T, growth also will be random as observed experimentally,[15,17] leading to rougher a-Si:H films covered with Si trihydrides that also are observed in experiments.[15] However, for $T>500$ K, the H-transfer reaction is expected to dominate as the primary Si incorporation event, leading to the formation of smooth a-Si:H films covered with Si dihydrides. For $T>650$ K, the Si dihydrides formed after H transfer from the SiH_3 radical can dissociate further on the a-Si:H surface, leading to the formation of Si monohydrides; such dissociation reactions have been observed in our MD simulations, and have been proposed on the basis of experimental observations.[29,30] In fact, experimental measurements using *in situ* attenuated total internal reflection Fourier transform infrared spectroscopy have revealed that the a-Si:H surface coverage is dominated by trihydrides at $T\sim300$ K, by dihydrides at $T\sim500$ K, and by monohydrides at $T>650$ K,[30] while the trihydride concentration decreases with increasing T.[29,30]

Furthermore, we do not expect DB diffusion from hills to valleys to be the key step that mediates the surface smoothening mechanism. The diffusion of DBs from hills to valleys occurs only when chemisorbed H atoms, i.e., H atoms that are bonded to fourfold coordinated Si atoms, diffuse from valleys to hills. The barrier for an H atom to break away from a DB in a-Si:H is in excess of 2.5 eV (Ref. 42) and would lead to DB diffusion only over time scales that are much longer than the SiH_3 radical diffusion and Si incorporation time scales captured in our MD simulations. In the MD simulations, we observe H-transfer events to be mediated by floating bonds, and, therefore, H-diffusion processes occurring over MD time scales do not result in DB diffusion.[41,43] Hence, the surface smoothening mechanism analyzed in this article is consistent with both the experimental data for a-Si:H surface roughness evolution and with the experimentally observed surface hydride compositions and low surface DB coverage.

VII. CONCLUSIONS

In summary, we have analyzed the fundamental radical precursor diffusion and incorporation processes that determine the surface smoothness of a-Si:H thin films, using molecular-dynamics (MD) simulations of radical precursor migration on surfaces of a-Si:H films, as well as first-principles density functional theory (DFT) calculations on the Si(001)-(2×1):H surface. The surfaces of these MD-grown amorphous films are remarkably smooth due to a valley-filling mechanism where the mobile precursor, the SiH_3 radical, diffuses and incorporates preferentially in surface valleys. Analysis of the MD simulations of SiH_3 radical migration on smooth a-Si:H surfaces yields an effective diffusion barrier of 0.16 eV. The low diffusion barrier on the a-Si:H surface is attributed to SiH_3 migration through overcoordinated surface Si atoms, where the radical remains weakly bonded to the surface at all times and does not break any strong Si-Si bonds along its migration pathway. The diffusing SiH_3 radical incorporates into the a-Si:H film only when it transfers an H atom and forms a second Si-Si back-

bond. On rough a-Si:H films, such H transfer from diffusing SiH_3 radicals is more likely to occur in surface valleys, even when the dangling bond (DB) density is low and DBs are not present in surface valleys. In addition, this H-transfer process is thermally activated, with a spectrum of activation energy barriers (E_a) over the range 0.29–0.65 eV. The preferential incorporation in valleys is explained by both the increased residence time of the migrating precursor in valleys and the decreased activation barrier for incorporation reactions occurring in valleys.

ACKNOWLEDGMENTS

This work was supported by the NSF/DOE Partnership for Basic Plasma Science and Engineering (Grant No. ECS-0317345), an NSF/ITR grant (Grant No. CTS-0205584), an NSF equipment grant (Grant No. CTS-0417770), and support from the Camille and Henry Dreyfus Foundation to one of the authors (D.M.). Fruitful discussions with E. S. Aydil and S. Agarwal are gratefully acknowledged.

*Corresponding author. Email address: maroudas@ecs.umass.edu

[1] A. Shah, P. Torres, R. Tscharner, N. Wyrsch, and H. Keppner, Science **285**, 692 (1999).
[2] C. Beneking, B. Rech, J. Foelsch, and H. Wagner, Phys. Status Solidi B **194**, 41 (1996).
[3] R. A. Gottscho, M. E. Barone, and J. M. Cook, MRS Bull. **21**, 38 (1996).
[4] A. Gallagher, J. Appl. Phys. **63**, 2406 (1988).
[5] R. Robertson and A. Gallagher, J. Appl. Phys. **59**, 3402 (1986).
[6] A. H. M. Smets, M. C. M. van de Sanden, and D. C. Schram, Thin Solid Films **344**, 281 (1999).
[7] D. A. Doughty, J. R. Doyle, G. H. Lin, and A. Gallagher, J. Appl. Phys. **67**, 6220 (1990).
[8] C. C. Tsai, J. C. Knights, G. Chang, and B. Wacker, J. Appl. Phys. **59**, 2998 (1986).
[9] S. Ramalingam, S. Sriraman, E. S. Aydil, and D. Maroudas, Appl. Phys. Lett. **78**, 2685 (2001).
[10] M. S. Valipa, S. Sriraman, E. S. Aydil, and D. Maroudas, Surf. Sci. **574**, 123 (2005).
[11] S. Yamasaki, U. K. Das, T. Umeda, J. Isoya, and K. Tanaka, J. Non-Cryst. Solids **266–269**, 529 (2000).
[12] T. Shimuzu, X. Xu, H. Kidoh, A. Morimoto, and M. Kumeda, J. Appl. Phys. **64**, 5045 (1988).
[13] W. M. M. Kessels, M. C. M. van de Sanden, and D. C. Schram, J. Vac. Sci. Technol. A **18**, 2153 (2000).
[14] K. R. Bray and G. N. Parsons, Phys. Rev. B **65**, 035311 (2002).
[15] A. H. M. Smets, W. M. M. Kessels, and M. C. M. van de Sanden, Appl. Phys. Lett. **82**, 865 (2003).
[16] A. J. Flewitt, J. Robertson, and W. I. Milne, J. Appl. Phys. **85**, 8032 (1999).
[17] M. Kondo, T. Ohe, K. Saito, T Nishimiya, and A. Matsuda, J. Non-Cryst. Solids **227–230**, 890 (1998).
[18] D. M. Tanenbaum, A. L. Laracuente, and A. Gallagher, Phys. Rev. B **56**, 4243 (1997).
[19] K. K. Gleason, K. S. Wang, M. K. Chen, and J. A. Reimer, J. Appl. Phys. **61**, 2866 (1987).
[20] K. Maeda, A. Kuroe, and I. Umezu, Phys. Rev. B **51**, 10635 (1995).
[21] R. Dewarrat and J. Robertson, Thin Solid Films **427**, 11 (2003).
[22] M. S. Valipa, E. S. Aydil, and D. Maroudas, Surf. Sci. **572**, L339 (2004).
[23] D. Maroudas, Adv. Chem. Eng. **28**, 251 (2001).
[24] S. Sriraman, Ph.D. thesis, University of California, Santa Barbara, 2003.
[25] T. Ohira, O. Ukai, T. Adachi, Y. Takeuchi, and M. Murata, Phys. Rev. B **52**, 8283 (1995).
[26] T. Ohira, O. Ukai, M. Noda, Y. Takeuchi, M. Murata, and H. Yoshida, Mater. Res. Soc. Symp. Proc. **408**, 445 (1996).
[27] S. Ramalingam, D. Maroudas, and E. S. Aydil, J. Appl. Phys. **84**, 3895 (1998).
[28] D. C. Marra, E. A. Edelberg, R. L. Naone, and E. S. Aydil, J. Vac. Sci. Technol. A **16**, 3199 (1998).
[29] D. C. Marra, W. M. M. Kessels, M. C. M. van de Sanden, K. Kashefizadeh, and E. S. Aydil, Surf. Sci. **530**, 1 (2003).
[30] E. S. Aydil, D. Maroudas, D. C. Marra, W. M. M. Kessels, S. Agarwal, S. Ramalingam, S. Sriraman, M. C. M. van de Sanden, and A. Takano, Mater. Res. Soc. Symp. Proc. **664**, A1.1 (2001).
[31] S. Sriraman, S. Agarwal, E. S. Aydil, and D. Maroudas, Nature **418**, 62 (2002).
[32] J. P. Perdew, K. Burke, and M. Ernzerhof, Phys. Rev. Lett. **77**, 3865 (1996).
[33] M. C. Payne, M. P. Teter, D. C. Allan, T. A. Arias, and J. D. Joannopoulos, Rev. Mod. Phys. **64**, 1045 (1992).
[34] D. Vanderbilt, Phys. Rev. B **41**, 7892 (1990).
[35] G. Henkelman, B. P. Uberuaga, and H. Jónnson, J. Chem. Phys. **113**, 9901 (2000).
[36] T. Bakos, M. S. Valipa, and D. Maroudas, J. Chem. Phys. **122**, 054703 (2005).
[37] A. Rahman, Phys. Rev. **136**, A405 (1964).
[38] M. S. Valipa, T. Bakos, E. S. Aydil, and D. Maroudas, Phys. Rev. Lett. **95**, 216102 (2005).
[39] T. Bakos and D. Maroudas, IEEE Trans. Plasma Sci. **33**, 230 (2005).
[40] S. Ramalingam, D. Maroudas, E. S. Aydil, and S. P. Walch, Surf. Sci. **418**, L8 (1998).
[41] S. Agarwal, M. S. Valipa, B. Hoex, M. C. M. van de Sanden, D. Maroudas, and E. S. Aydil, Surf. Sci. **598**, 35 (2005).
[42] B. Tuttle and J. B. Adams, Phys. Rev. B **57**, 12859 (1998).
[43] M. S. Valipa and D. Maroudas, Appl. Phys. Lett. **87**, 261911 (2005).
[44] Y.-S. Su and S. T. Pantelides, Phys. Rev. Lett. **88**, 165503 (2002).